Droplet size distribution measurements using phase-Doppler anemometry and shadowgraphy: Quantitative comparison

Ralf Kapulla[*], Mathias Trautmann[**], Alicia Hernandez Sanchez[***], Salvador Calvo Zaragoza[***], Sarah Hofstetter[****], Christoph Häfeli[****] and Salih Güntay[*]

[*] Laboratory for Thermal Hydraulics, Paul Scherrer Institut, 5232 Villigen, Switzerland.

[**] Studsvik GmbH & Co. KG, Hauptstrasse 1B, 76297 Stutensee, Germany

[***] Chemists Faculty, University of Murcia, Campus of Espinardo, 30100, Murcia, Spain.

[****] University of Applied Sciences Northwestern Switzerland, Institut of Automation, Aarauerstrasse 36, 5200 Brugg

Abstract

Water sprays with droplet size spectra in the range from 1 to 70 μm have been measured with a phase-Doppler-anemometer (PDA) and a direct imaging technique (shadowgraphy). The results of both systems are compared with respect to the count mean diameter $D(1,0)$ and geometric standard deviation σ_g. An image preprocessing is introduced (i) to account for non-uniform background illumination rendering previously recorded reference images negligible, (ii) to account for mean intensity fluctuations in images for situations where the light source is not temporally stable and (iii) to reject images with no particles, since picture of this type might spoil the subsequent analysis. It was found that the shadowgraphy-based $D(1,0)$ agrees within $+10\%$ / -0% with the PDA-based measurements, thus, the shadowgraphy based $D(1,0)$ is systematically larger. The broadness of the distributions characterised by σ_g deviate from each other by $+5\%$ / -15%, indicating that the out-of-focuse correction introduced for the shadowgraphy system needs refinement.

1 Introduction

Aerosol transport through complex geometries is a topic relevant to numerous industrial applications, for example in the steam generator (SG) of a nuclear plant during certain accident sequences, (Güntay et al. 2004). In order to determine the transport and the retention behavior of droplets, the droplet size distribution has to be determined in various SG components. Consequently the data characterizing location and spread of the distributions – count mean diameter, $D(1,0)$, count median diameter, $D(0,0)$ and geometric standard deviation σ_g – obtained from the available optical measurement systems, i.e. a phase Doppler anemometer (PDA) and a direct imaging technique necessitates an inter-comparison. These techniques are based on different sizing principles which makes careful interpretation of the results mandatory. Therefore experiments were conducted with water droplets in the range from 1 to 70 μm, $D(1,0)$. A pair of tests, each utilizing one optical system, was conducted under identical boundary conditions.

2 Experimental-Setup

The water droplets for both measurement series using PDA- and Shadowgraphy systems were generated with a two-fluid atomization, air-assist, full cone spraying nozzle projecting upwards. To obtain different drop-size spectra, the operation conditions of the spraying nozzle have been

air volumetric flow rate (FL) $l/\min$	water flow rate (FW) l/h 0.5	water flow rate (FW) l/h 1.0	water flow rate (FW) l/h 1.5	water flow rate (FW) l/h 2.5
10	✓	✓	✓	✓
30	✓	✓	✓	✓
50	✓	✓	✓	✓

Table 1: *Operation conditions for the spraying nozzle.*

varied according Table 1. The measurement location for both systems was placed in the axis at an axial distance of $10\ mm$ from the nozzle orifice.

The phase-Doppler measurements have been performed by means of a three-detector, standard DANTEC PDA. Since we will focus on the shadowgraphy system, the operation principles of the PDA can be found elsewhere, (Albrecht et al. 2003). The relevant parameters of the PDA set-up are given in Table 2. The so-called 'Gaussian beam effect' as well as the 'slit-effect', see (Albrecht et al. 2003),pp. 466, has been considered. The former effect becomes important for droplet diameters above $\approx 70\ \mu m$ and the latter above $\approx 100\ \mu m$. For the present experiments, therefore, both effects can be neglected.

Laser	$ArIon$	$-$	focal length, receiver	310	mm
wavelength	514.5	nm	off-axis angle Φ	50	$^\circ$
laser power	20	$mW/beam$	aperture mask	$type\ A$	$-$
focal length, transmitter	800	mm	signal level validation	-2	dB
intersection angle $\Theta/2$	2.765	$^\circ$	high voltage level	$700-1200$	V
beam expander ratio	1.950	$-$	Dominating scattering order	refraction	$-$
probe volume dx	0.122	mm	Phase conversion	$2.989, 1.494$	$^\circ/\mu m$
probe volume dy	0.122	mm			
probe volume dz	2.578	mm	BSA Flow Software	$V4.11$	

Table 2: *Optical parameters used for the measurements.*

Since operation parameters such as laser power, photomultiplier amplification voltage and signal gain, can significantly influence the results, i.e. the measured mean diameter and the broadness of the distribution, these parameters have been determined for each particle batch individually in the asymptotic range as recommended in (Kapulla and Najera 2006), to ensure that the result is independent of the operation parameters.

The hardware for the shadowgraphy equipment consists of a non-coherent double-pulsed laser backlight (Nd:YAG laser, Quantel Brilliant Twins B, Energy 380 mJ, pulse duration $5\ ns$) which illuminates the particles passing the system between the light source and CCD camera (PCO Sensicam, 12 bit, pixel size $6.45\ \mu m^2$, Resolution 1376x1040 pixel). The camera can be equipped with a long distance microscope (Questar QM-1, working distance 560 to $1520\ mm$) and optional additional magnification lenses, Fig. 1. After calibration each pixel represents an area of $0.907\ \mu m^2$ in the object-plane. The double-pulsed laser allows the recording of short-time-separated pictures and therefore also the calculation of droplet velocities with particle tracking algorithms, but this topic is beyond the scope of this article.

The analysis of the images is a 4-stage process. The first step consists in image pre-processing operations, the second step in separating and detecting the different droplets on each picture, the third step in calculating the droplet size and the fourth step in different filter operations for the particles detected. For the complete analysis chain the software Davis (V7.2.1, LaVision) was used where the major non-standard part of the pre-processing algorithms was programmed with the included C-like command language.

Despite careful adjustment of the beam alignment, the mean image intensity within each frame of a double picture (i) remained constantly different, (ii) varied with time for short time scales and (iii) were non-stable for large time scales, Fig. 2 a).

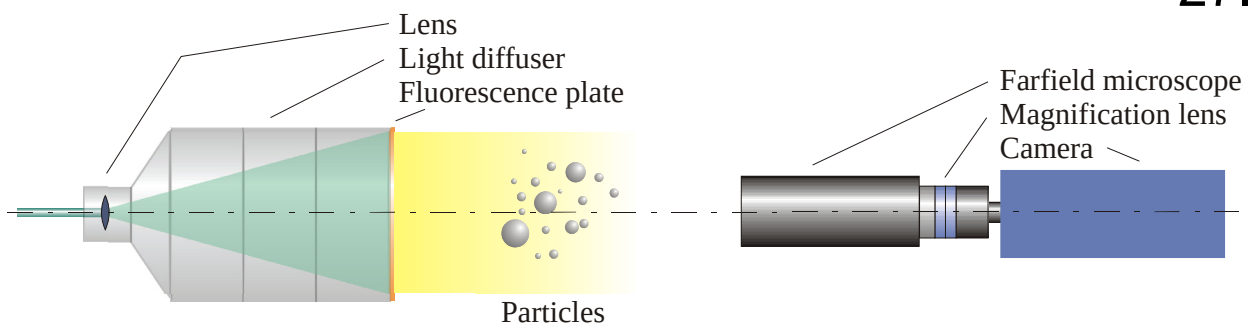

Figure 1: *Backlight illumination and camera set-up for for the Shadowgraphy system used.*

To correct for these effects, each picture of a series was separated into its two frames and the mean intensity of each frame was shifted to an arbitrarily chosen reference value identical for all frames, Fig. 2 b). Experiences with the DaVis software revealed that the particle detection most probably failed for pictures with small differences between the maximum and minimum intensity in one frame, $I_{\max} - I_{\min}$, Fig. 2 b). The darkest pixel, $I_{\min}$, – arbitrarily located – is caused by droplet-shadows, whereas the brightest pixel, $I_{\max}$, is always located in the frame centres since – although diffused – the initial Gaussian-like distribution of the laser beam is not completely lost. Additionally, the gray value in the shadow picture of *small droplets* results in higher grey values compared with *bigger droplets*, (Blaisot and Yon 2005). This explains the much higher RMS-value for $I_{\min}$ compared with that of $I_{\max}$. Overall, imaging the spraying process results in few pictures with no particles, region A in Fig. 2 b), pictures with a combination of smaller and bigger particles, region B and few pictures with big particles, region C. Therefore, a small $I_{\max} - I_{\min}$ indicates pictures with no, with only few, very small or defocused particles. To remove these pictures a threshold value is calculated with $I_{thresh} = \overline{I}_{\min} + I_{\min,rms} - p \cdot I_{\min,rms}$ where the mean of the minimum intensity is denoted by $\overline{I}_{\min}$, the corresponding RMS-value by $I_{\min,rms}$ and a user selectable adjustment parameter by p. Pictures with $I_{\min} > I_{thresch}$ are excluded from the analysis, Fig. 2 b).

Since the background illumination of the pictures is rarely uniform, the raw image, G_{raw}, is subtracted pixel by pixel from a reference image, G_{ref}, and the resulting image, G', is called the inverted image, since the formerly dark droplet shadows appear in white, Fig. 3. The large-scale Gaussian background intensity is removed and the droplet shadows appear now as intensity peaks

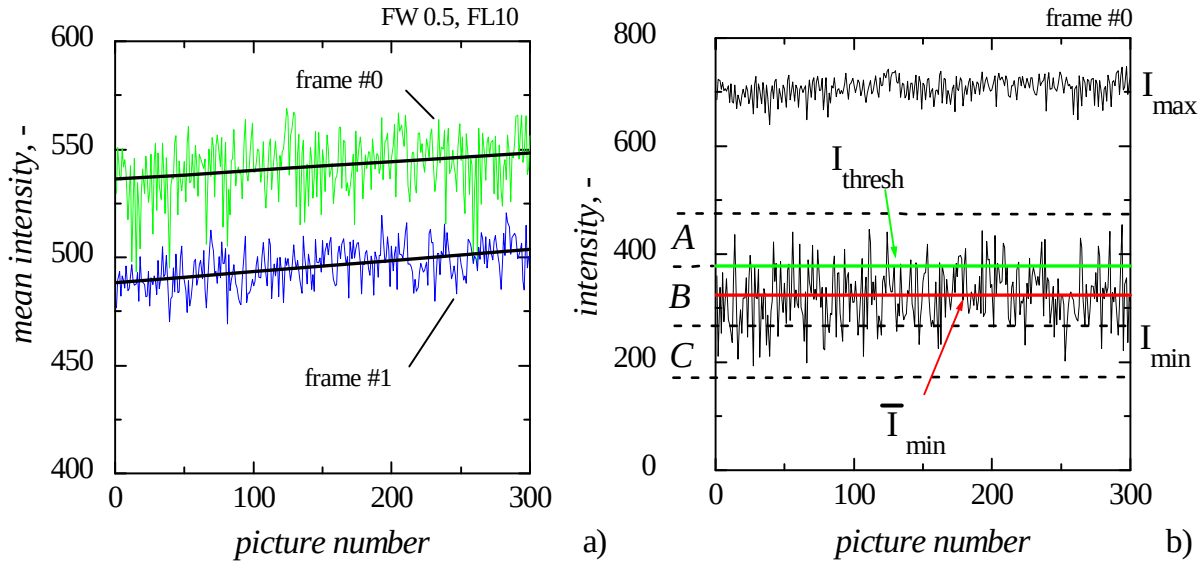

Figure 2: *Mean intensity of both frames of a double-pulsed image as a function of time (left) and minimal and maximal intensity for one intensity shifted frame over time (right).*

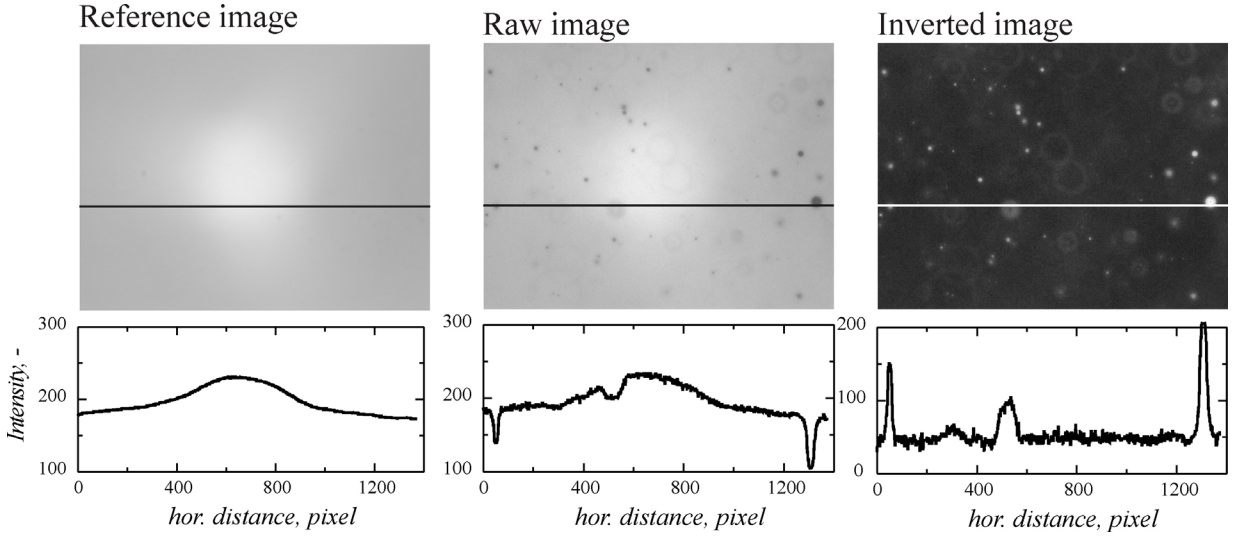

Figure 3: *Effect of the inversion the raw image with a reference image.*

over a spatially fairly homogeneous background. Image G_{ref} was obtained by simply averaging all the raw pictures of a measurement series. To separate the shadow-images of the droplets from the background, a classical, global threshold approach at a given level, L_{th}, is used. Since further analysis-steps to extract the droplet sizes are explained in the Davis Manual, we will highlight subsequently only those topics relevant for the comparison with PDA results in the following section.

3 Results

For all the experiments and for both systems, the measured size distributions of the droplets show a log-normal shape. As an example, the probability density functions (PDF) for the droplet-size distributions are compared in Fig. 4 a). It is found that location, spread and shape of both distributions measured with the different devices agree very well. Additionally, (i) to compare the results with the literature and (ii) to test for the consistency of the data, the volume mean diameter, $D(3,3)$ and the Sauter mean diameter, $D(3,2)$, were calculated directly from the par-

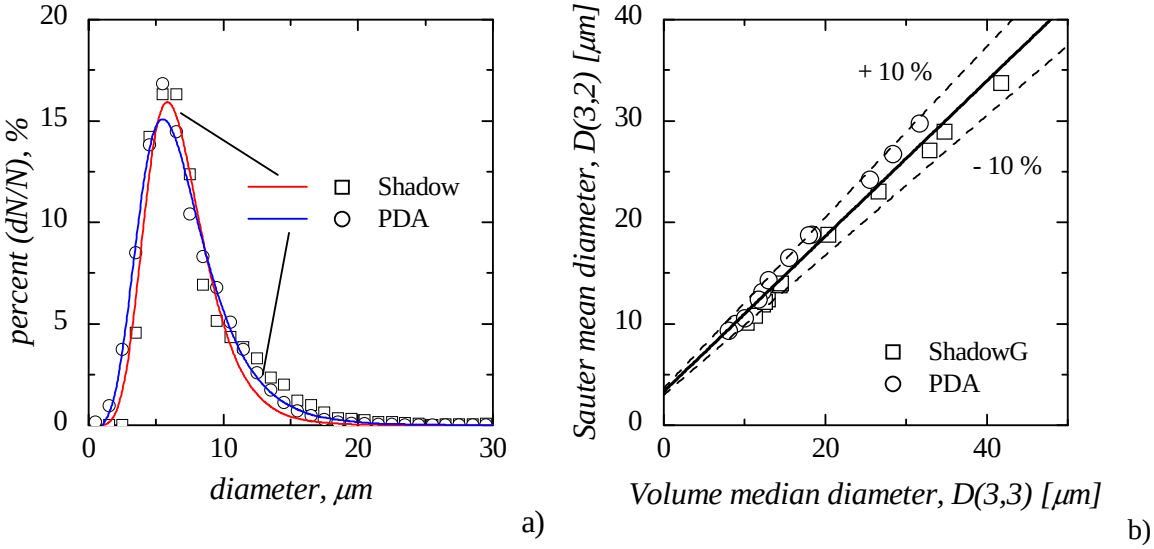

Figure 4: *Comparison of droplet size distribution measured with PDA and shadowgraphy systems, Test: FW = 0.5 l/h, FL= 30 l/min (left) and correlation of volume median diameter, $D(3,3)$, and Sauter mean diameter, $(D3,2)$, for all operational parameters of the spraying nozzle according Table 1 (right).*

ticle lists and correlated as suggested by (Simmons 1977). The resulting points were fitted to a straight line from which $D(3,3)/D(3,2) = 1.3$ as a mean value and almost all points fall within ± 10 % of this mean, Fig. 4 b). For comparison purposes: (Simmons 1977) results are representative of hundreds of tests with different nozzles and operational parameters and he found $D(3,3)/D(3,2) = 1.2$ and the points falling within ± 5 % which is in good agreement with our results. Previous measurements with latex spheres have shown that we apparently touch the lower resolution limit with particles corresponding to 25 Pixel, (Kapulla et al. 2006). Using the calibration, a droplet with diameter of $5\ \mu m$ corresponds to approximate 25 pixel in the image plane. We therefore rejected particles below 25 pixel from the shadowgraphy-based distribution. Therefore, subsequent statistical results for PDA have been calculated with droplets below $5\ \mu m$ being also excluded. Conversely, due to the sphericity-assumption of the PDA, the centricity criteria for the shadowgraphy system was set to 80 %, i.e. the ratio of the longest and shortest particle axis must be above 80%, therefore rejecting non-spherical particles. Additionally, a local threshold criteria was applied to reject – implicitly – out-of-focus particles by assessing the boundary gradient of the shadow pictures. Furthermore, the out-of-focus problem is considered. The out-of-focus phenomenon denotes the fact that an unfocused droplet seems to be larger than a focused one of the same size, (Blaisot and Yon 2005). Unfortunately, the depth-of-field is size dependent, i.e. bigger droplets have larger depth-of-fields than smaller ones. Accounting of out-of-focus particles therefore preferentially rejects smaller droplets which implies an overestimation of bigger droplets. To compensate for this bias and since the diameter/depth-of-field relation can be approximated by a straight line, (Kim and Kim 1994), the resulting droplet size distribution can be corrected with $p = D(1,0)/D_{ref}$ where p is the probability to detect at particle with size D and the reference diameter D_{ref} equals the largest detected particle ensuring that p is below 1. The amount of particles are then re-evaluated with $1/p$ and the statistics are corrected. Additionally a border correction is applied, since – for a given field-of-view – the probability of detecting a larger droplet is smaller than for a smaller droplets.To further quantify the agreement between the PDA- and shadowgraphy-based results, the count mean diameter and $D(1,0)$ and the count median diameter, $D(0,0)$ are additionally calculated directly from the particle lists. The geometric standard deviation σ_g was obtained by fitting the PDF to:

$$PDF(d_p) = \frac{A}{\sqrt{2\pi}\ln(\sigma_g)\cdot d_p}\exp\left\{-\frac{(\ln(d_p)-\ln(D(0,0)))^2}{2\cdot\ln^2(\sigma_g)}\right\} \quad (1)$$

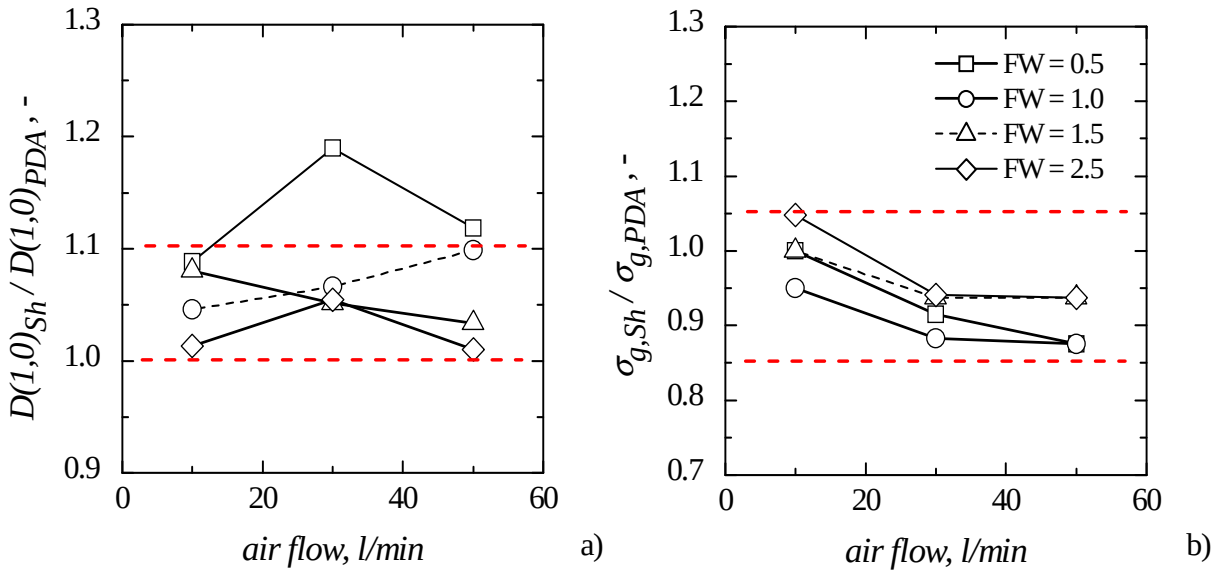

Figure 5: *Comparison of PDA-based and shadowgraphy-based count mean diameter (left) and the corresponding geometric standard deviations as a function of air-flow with the water flow as parameter..*

where the geometric standard deviation (GSD) defined as $\sigma_g = (d_{84\%}/d_{16\%})^{1/2}$ characterizes the spread of the distribution, while the count median diameter ($D(0,0)$) characterizes the diameter for which $50\,\%$ of the total number of particles are smaller. The amplitude A has been introduced, since the PDFs have not been normalized with the size of the diameter classes. Subsequently, the PDA-based measurements are denoted with index PDA and the shadowgraphy based with index Sh. Arbitrarily the PDA-based results are attributed as the reference, therefore we calculated the fractions $D(1,0)_{Sh}/D(1,0)_{PDA}$ as well as $\sigma_{g,Sh}/\sigma_{g,PDA}$. The results can be found in Fig. 5. For 11 out of 12 experiments, the $D(1,0)$ agrees within $^{+10\,\%}_{-0\,\%}$ of one another determined by both systems, Fig. 5 a). It is noteworthy that the shadowgraphy-based $D(1,0)$ is always larger than the PDA-based $D(1,0)$, which might indicate that the amount of smaller particles introduced by the out-of-focus criteria are underestimated and that the criteria, therefore, needs special attention for the future. There seems to be no systematic relation between either the water or the air flow rate and $D(1,0)_{Sh}/D(1,0)_{PDA}$. There is one outlier for parameters $FL = 30$ $l/\min$ and $FW = 0.5\,l/h$. Despite careful re-calculation of the results no obvious error could be detected. The calculated spread of the distributions, Eq. 1, are within $^{+5\,\%}_{-15\,\%}$ of one another , Fig. 5 b). There is a systematic relation between the air flow rate and $\sigma_{g,Sh}/\sigma_{g,PDA}$. For increasingly higher air flow rates – associated with a smaller distribution – the shadowgraphy system seems to underpredict the broadness of the distribution. This might be the result either of the amount of detected smaller particles being too small or the amount of bigger droplets being too small – or both. The latter cause is very unlikely, since the detectability of larger droplets is much better than that for smaller ones, whereas the former cause coincides with the probable underestimation of the out-of-focus correction with respect to smaller particles stated above.

4 Summary

All distributions show a log normal shape and the location, $D(1,0)$, and spread parameter, σ_g, obtained from both techniques agrees with $^{+10\,\%}_{-0\,\%}$ and $^{+5\,\%}_{-15\,\%}$, respectively. The shadowgraphy-based $D(1,0)$ is always larger than the PDA-based which might indicate that the ammount of smaller particles introduced by the out-of-focus criteria is underestimated, therefore, the out-of-focus criteria needs special attention for future measurements. For smaller size distributions the shadowgraphy system tends to underpredict the spread of the distribution.

References

Albrecht, H.-E. and Borys, M. and Damaschke, N. and Tropea, C. (2003). Laser doppler and phase doppler measurement techniques. Springer-Verlag.

Blaisot, J.B., Yon, J. (2005), Droplet size and morphology characterization for dense sprays by image processing: applications to the Diesel spray, Experiments in Fluids, Vol. 39, pp. 977-994.

Güntay, S., Suckow, D., Dehbi, A., Kapulla, R, (2004), ARTIST: introduction and first results, Nuclear Engineering and Design, Vol. 231, pp. 109-120.

Kapulla, R. and Najera B. (2006), Sensitivity Assessment of a Phase-Doppler Interferometer to User-Controlled Settings, Meas. Sci. Technol. 17, pp. 221–227.

Kapulla, R., Trautmann, M., Güntay, S., Dehbi, A. and Suckow, D. (2006), Comparison between phase-Doppler anemometry and shadowgraphy systems with respect to solid-particle size distribution measurements, Lasermethoden in der Strömungsmesstechnik, 14. Fachtagung, Braunschweig.

Kim, K.S. and Kim, S.S. (1994), Drop sizing and depth-of-field correction in TV imaging, Atomization and Sprays, vol. 4, pp. 65-78.

Simmons, H.C. (1977), The correlation of drop-size distributions in fuel nozzle sprays, Journal of Engineering for power, 99, pp. 309-314.